Quantum Vacuum Excitation of a Quasinormal Mode in an Analog Model of Black Hole Spacetime

M. J. Jacquet[1,*] L. Giacomelli[2] Q. Valnais[1] M. Joly,[1] F. Claude,[1] E. Giacobino,[1]
Q. Glorieux[1] I. Carusotto,[2] and A. Bramati[1]

[1]*Laboratoire Kastler Brossel, Sorbonne Université, CNRS, ENS-Université PSL, Collège de France, Paris 75005, France*
[2]*INO-CNR BEC Center and Dipartimento di Fisica, Università di Trento, via Sommarive 14, I-38123 Povo, Trento, Italy*

Vacuum quantum fluctuations near horizons are known to yield correlated emission by the Hawking effect. We use a driven-dissipative quantum fluid of microcavity polaritons as an analog model of a quantum field theory on a black-hole spacetime and numerically calculate correlated emission. We show that, in addition to the Hawking effect at the sonic horizon, quantum fluctuations may result in a sizable stationary excitation of a quasinormal mode of the field theory. Observable signatures of the excitation of the quasinormal mode are found in the spatial density fluctuations as well as in the spectrum of Hawking emission. This suggests an intrinsic fluctuation-driven mechanism leading to the quantum excitation of quasinormal modes on black hole spacetimes.

Quantum fluctuations of fields in the vicinity of the event horizon of black holes (BHs) are predicted to cause the emission of correlated waves by the Hawking effect (HE) [1]: while Hawking radiation propagates away from the horizon to outer space, the partner radiation falls inside the horizon. Since signaling from inside the horizon is impossible, only the out-going Hawking radiation is observable and quantum correlations with the in-falling partner waves cannot be accessed.

The HE may also be observed in the laboratory thanks to analog gravity setups [2,3], namely, condensed matter or optical systems, engineered in such a way that their collective excitations propagate on effectively curved spacetimes [4,5]. This idea has been experimentally demonstrated in a variety of platforms [6–18]: for example, a horizon for sound waves forms in a one-dimensional transsonic fluid where the flow velocity of the fluid exceeds the speed of sound. Crucially, observation on both sides of the horizon is possible with analog setups and the HE has been detected via density correlations between Hawking radiation and its partner [19,20] in experiments based on both classical [21] and quantum fluids [22].

In this Letter, we make use of a specific realization of an effective spacetime realized in a driven-dissipative quantum fluid of exciton polaritons in a semiconductor microcavity [11,23–25] to push forward the theoretical study of quantum fluctuations in the vicinity of horizons. In particular, we investigate a one-dimensional transsonic configuration where the spatial shape of the quantum fluid and the external potential are optimized together to maximize the strength of the HE [26]. We find that the typical signatures of the HE are supplemented by new features in the spatial correlation of sound waves that evidence the

coupling of propagating waves to a localized mode living near the horizon, namely, a quasinormal mode (QNM) of the acoustic field. On a curved spacetime with a horizon, QNMs are decaying solutions of the Klein-Gordon equation of the field satisfying purely in-(out-)going boundary conditions at the horizon (at infinity) [27,28] and correspond to the intrinsic oscillation modes of generic fields in BH spacetime [29]. Typically, localized modes have a finite lifetime due to radiative decay into waves propagating away from the horizon, for instance gravitational waves [27,28].

While classical ringdown oscillations of a scalar field have been observed experimentally for surface waves in a rotating bathtub flow configuration [30] and a structured HE spectrum has been theoretically calculated in more complex flow geometries in conservative fluids [31], our work establishes that QNMs of quantum fields get naturally excited by the same quantum fluctuations that are responsible for the HE. Translated back to the astrophysical context, our results suggest a general and intrinsic fluctuations-driven mechanism leading to quantum excitation of BH spacetimes.

Effective spacetime in a polariton fluid.—Our numerical study is based on the parameters of the system used in the experiment [11]: we consider a 800 μm long wire (a GaAs-based semiconductor microcavity embedding one InGaAs quantum well) within which the polariton dynamics is effectively one dimensional. There is an attractive defect formed by a 1 μm long broadening of the wire halfway along it at $x_d = 0$, cf. Fig. 1(a).

The device is excited with a continuous wave laser (the pump) incident at a finite angle with respect to the normal to form a continuous flow of polaritons along the wire. The pump frequency ω_p is tuned above the bare polariton
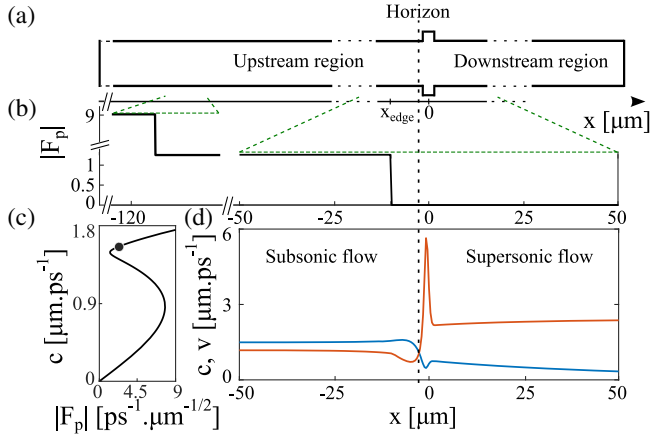
FIG. 1. Properties of the transsonic polariton fluid flow. A steplike laser field pumps polaritons, creating a transsonic fluid flow across an attractive obstacle. (a) Sketch of the polariton wire with a defect at $x_d = 0$. (b) Spatial profile of the pump near the defect. The pump intensity $|F_p|[\text{ps}^{-1} \mu\text{m}^{-1/2}]$ drops abruptly to 0 at $x_{\text{edge}} = -10 \mu\text{m}$. (c) Optical bistability of the spatially homogeneous polariton fluid. (d) Spatial properties of the stationary fluid near the defect: orange, fluid velocity v; blue, speed of excitations c.

resonance ω_0 at the pump wave number k_p to enforce a regime of optical bistability between the pump strength $|F_p|$ and the density of the fluid n [32,33], see Fig. 1(d) where we plot the speed of excitations $c = \sqrt{\hbar g n / m^*}$, as a proxy of the polariton density n (g is the interaction strength and m^* is the polariton mass). The pump spot is structured in a two-step profile: on the first step, the fluid is set above the bistable regime ($|F_p| = 9 \text{ ps}^{-1} \mu\text{m}^{-1/2}$) on the second step the fluid density is supported near the turning point of the bistability loop [$|F_p| = 1.2 \text{ ps}^{-1} \mu\text{m}^{-1/2}$, see black dot on Fig. 1(c)] over about 100 μm up until the sharp pump edge $x_{\text{edge}} = 10 \mu\text{m}$ [cf. Fig. 1(b)].

In the region $x < 0$, the phase θ of the fluid is locked to that of the pump, with a velocity $v = (\hbar/m^*)\partial_x \theta$ in the positive x direction. In the region $x > 0$, polaritons propagate ballistically with an exponentially decaying density and a finite velocity [34]. Figure 1(d) shows the fluid velocity v in orange and the speed of excitations c in blue. The acoustic horizon separating the upstream subsonic ($v < c$) region from the downstream supersonic ($v > c$) region is clearly visible at $x_H = -3 \mu\text{m}$.

Excitations of a homogeneous fluid obey the k-dependent Bogoliubov dispersion relation $\omega = \pm\sqrt{\hbar k^2/2m^{*2}(\hbar k^2/2m^{*2} + 2gn)} + vk - i\gamma/2$, which depends on both v and n as well as on the particle loss rate γ. It depends on the working point along the bistability loop and when driven, as in the upstream region, may be slightly gapped [33]. Figure 2 shows the dispersion in the asymptotic regions (a) up- and (b) downstream from the horizon. The blue (orange)
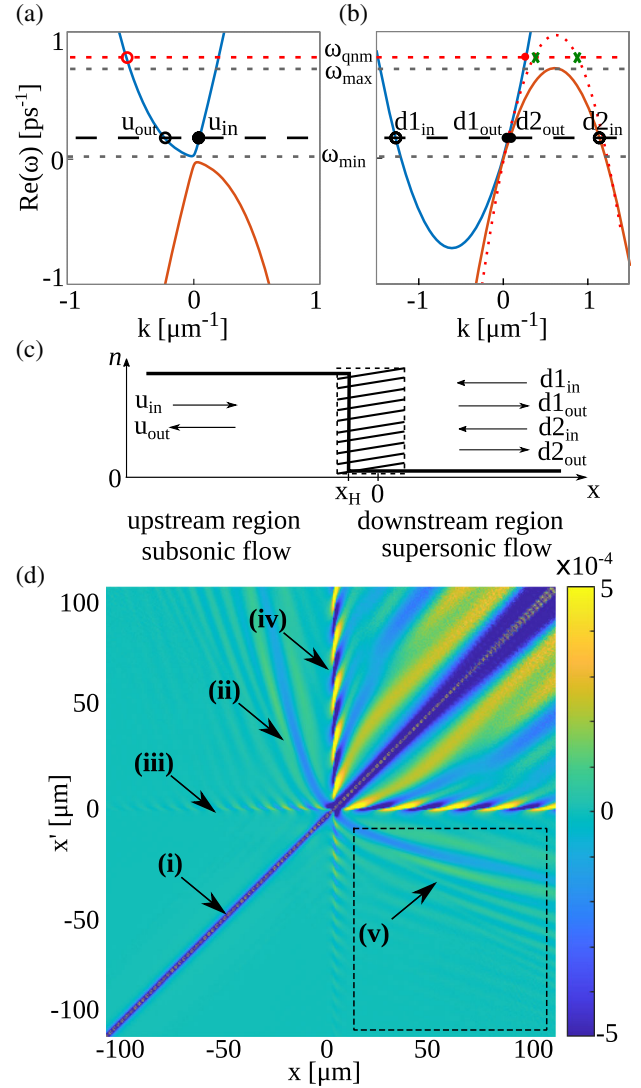
FIG. 2. Modes and correlated emission. (a),(b) Bogoliubov dispersion relation in the asymptotic regions as seen from the laboratory frame. (a) Subsonic fluid flow. (b) Supersonic fluid flow. Blue line, positive-norm modes; orange line, negative-norm modes; red dashed line, behavior of the negative-norm branch in the highly supersonic region. Circles (filled dots), asymptotic modes of negative (positive) group velocity. Gray dashed lines, $\omega_{\min}$ and $\omega_{\max}$; red dashed line, ω_{QNM}; black dashed line a generic frequency giving to the mode structure of (c). (c) Modes of the system in the laboratory frame. Schematic of the fluid density in the asymptotic regions (the dashed region has extra structure) and asymptotic mode structure on either side of the horizon. (d) Normalized spatial correlations $g^{(2)}(x, x') - 1$. Traces: (i) antibunching; (ii) Hawking mustache; (iii) QNM and Hawking radiation; (iv) QNM and witness mode; (v) modulation of the Hawking mustache by QNMs.

curve represents positive- (negative-)norm modes of the field, respectively [35]. In the upstream region, the pump strength is tuned slightly above the turning point of the bistability loop to keep the system stable on the upper

branch [26]: this introduces a small gap of size $\omega_{\min}$ between the positive- and negative-norm modes in the upstream region. As $v < c$, the Doppler shift is small and the positive- (negative-)norm modes remain at positive (negative) frequencies. In the downstream region of ballistic flow, the dispersion recovers the gapless Bogoliubov dispersion of conservative atomic condensates. As $v > c$, the large Doppler effect pulls negative-norm modes to positive frequencies up to $\omega_{\max}$.

As is typical in analog systems based on quantum fluids, the description of collective modes in terms of an effective metric on a curved space-time is only valid for small k modes [35–38]. For larger wave numbers, the superluminal form of the dispersion allows sound waves to propagate against the supersonic fluid flow in the downstream region. The combination of the superluminal correction of the dispersion and the Doppler effect is, in fact, what enables the mixing of positive- and negative-norm modes at the horizon for frequencies within the interval $[\omega_{\min}, \omega_{\max}]$.

Hawking effect.—This mode mixing at the horizon is the HE, i.e., the conversion of quantum fluctuations in the ingoing $\{u_{\text{in}}, d1_{\text{in}}, d2_{\text{in}}\}$ modes propagating towards the horizon into pairs of real excitations in the out-going $\{u_{\text{out}}, d1_{\text{out}}, d2_{\text{out}}\}$ modes [cf. Fig. 2(c)] [35,36]. The correlated nature of the emission is visible in the intensity correlation diagram shown in Fig. 2(d), where the normalized correlation function $g^{(2)}(x, x')$ of density fluctuations (computed with the truncated Wigner method [39] as a statistical average over 10^9 Monte Carlo realizations) is plotted as a function of the positions x, x'. Here, besides the trivial antibunching (i) along the $x = x'$ diagonal stemming from repulsive interactions, the usual signature of HE is apparent as a 100 µm-long oblique "mustache" of relative amplitude $\approx 10^{-3}$ (ii) due to correlations across the horizon between Hawking radiation (u_{out}) and the witness ($d1_{\text{out}}$) and partner ($d2_{\text{out}}$) modes in the downstream region.

Localized correlation features.—In addition to these typical features of the HE, the correlation plots of Fig. 2(d) reveal new structures: (iii) a series of oblique interference fringes developing along the $x = 0$, $x' > 0$ half line (and symmetrically along the $x' = 0$, $x < 0$ half line), and (iv) a similar, stronger series of oblique fringes localized along the $x = 0$, $x' > 0$ half line (and symmetrically along the $x' = 0$, $x > 0$ half line). These traces indicate correlations between excitations in a mode spatially localized near the horizon and waves propagating in either the upstream (iv) or the downstream (iii) regions. The spacing of the fringes yields the wave number of the propagating modes [see Supplemental Material (SM) [40]]: $|k_u| = 0.78(1)$ µm^{-1} and $|k_d| = 0.25(3)$ µm^{-1} in the up- and downstream region, respectively. Via the dispersion relation, $k_{u,d}$ correspond to the same frequency $\omega_{\text{QNM}} \sim 0.75$ ps$^{-1} > \omega_{\max}$ indicated by the red dashed line in Figs. 2(a) and 2(b), and to modes u_{out} and $d1_{\text{out}}$ that both have a positive norm. This single frequency indicates that we observe a single mode of the

acoustic field, composed of a localized component coupled to propagating waves on either side of the horizon.

Ringdown of the acoustic field.—The temporal dynamics of these coupled modes are not resolved by the equal-time correlation diagram Fig. 2(d) which displays the stationary properties of the emission. To assess these dynamics, we simulate the temporal evolution of the acoustic field upon perturbation by a probe. Figure 3 shows the temporal evolution of the spatial density profile of the fluid in response to a generic wave packet impinging on the horizon from the upstream $x < 0$ region. After the impinging wave packet has been partially reflected (i) and transmitted (ii) by the horizon, a long-lived oscillation persists in the region near the horizon (iii): here, the acoustic field undergoes ringdown oscillations at the frequency ω_{QNM}, with a lifetime $1/\gamma_{\text{QNM}} \approx 14$ ps about the same as the bare polariton lifetime $1/\gamma$. The coupling of the localized mode with the propagating (iv) u_{out} and (v) $d1_{\text{out}}$ modes in the up- and downstream region, respectively, is also visible in Fig. 3.

This kind of ringdown is typical of the oscillation of QNMs of fields on curved spacetimes upon short perturbations [28]. This oscillation occurs at the natural frequency of the underlying spacetime, independently of the details of the perturbation (as in BH merging for example [41]). This is also the case here as the signatures of the ringdown are robust against variations in the properties of the impinging wave packet, e.g., its frequency ω_{WP} (there is a resonance when $\omega_{\text{WP}} = \omega_{\text{QNM}}$). The real part of the frequency ω_{QNM} as well as the wave numbers $k_{u,d}$ obtained here are the same as those extracted from features (iii) and (iv) in the correlation diagram of Fig. 2(d), confirming that the
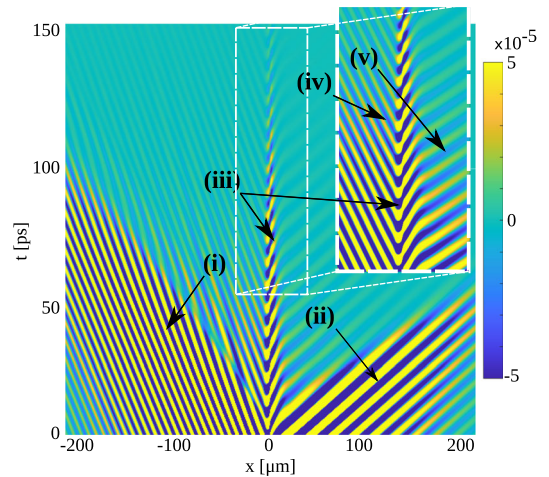
FIG. 3. Temporal evolution of the fluid density in response to an incident wave packet. $x_H = -3$ µm. Fluid density variation after excitation by a wave packet ($\Delta k_{\text{WP}} = 0.1$ µm^{-1}, carrier frequency $\omega_{\text{WP}} = \omega_{\text{QNM}}$) hitting the horizon at $t = 0$. Traces: (i) reflected wave, (ii) transmitted wave, (iii) state bound to the horizon, (iv) mode propagating upstream, (v) mode propagating downstream.

same QNM is responsible for both the ringdown and these features.

Physical origin of the QNM.—As can be seen in Fig. 1(c), the fluid density displays a marked dip. This dip is located in the inner region immediately after the horizon and is surrounded by two regions of different fluid density, forming an effective resonator for the Bogoliubov modes. Because of approximate conservation of the current, the density dip is accompanied by a narrow spike in the flow velocity v leading to a narrow region of highly supersonic flow. This is responsible for a large Doppler shift of the Bogoliubov modes, which, in particular, pulls the negative-norm branch to highly positive frequencies above ω_{max} [red-dotted curve in Fig. 2(b)]. Inside the resonator, negative-norm modes experience an effectively attractive potential [42] that pins their wave number [green crosses in Fig. 2(b)], creating a standing-wave-shaped localized mode of frequency ω_{QNM}. This localized negative-norm mode tunnel couples out into the propagating positive-norm modes u_{out} and $d1_{out}$ in the asymptotic up- and downstream region, respectively [red circle and dot in Fig. 2(b)]. This is confirmed by a direct diagonalization of the inhomogeneous Bogoliubov problem, as discussed in the SM.

Quantum excitation of the QNM.—This tunnel coupling between modes of opposite norm sign leads to the parametric amplification of vacuum fluctuations. In our configuration, the interfaces of the narrow resonator inside the horizon have a reflection coefficient effectively larger than unity for negative-norm waves: while this suggests that the field amplitude inside the resonator should grow exponentially, in our driven-dissipative fluid the instability is suppressed by the overall decay of the Bogoliubov modes due to the finite polariton lifetime [33], making the system dynamically stable. Similarly to parametric amplifiers driven below the instability threshold [43], the parametric process is responsible for a sizable steady-state excitation of the QNM via the spontaneous parametric emission of paired excitations in the localized mode and in the propagating u_{out} and $d1_{out}$ modes.

While the dynamical stability of the polariton fluid strongly depend on particle losses, the vacuum excitation of QNMs does not. In fact, the same phenomenon can also be observed with a conservative fluid. For example, in the SM we propose a toy-model configuration displaying an effective resonator near the horizon of a transsonic atomic BEC and show that such a system can be dynamically stable and display a QNM at $\omega_{QNM} < \omega_{max}$ that acquires a steady-state population with a clear signature in the correlation diagram of density fluctuations as well. These results confirm that our predicted effect is generic to fluid-based analog models. While damping is the crucial ingredient for a steady-state quantum vacuum excitation, it may have different origins depending on the driven-dissipative (particle losses) or conservative nature of the fluid (radiative decay into propagative waves on either side of the horizon).

Spectral modulation of correlated emission.—We obtain the spectrum of correlated emission via a two-dimensional Fourier transform (FT) of the spatial correlations $g^{(2)}(x, x')$ [44–47]. The contribution of the horizon region is suppressed by restricting the FT to the subspace delineated by the black dashed rectangle in the south-east quadrant in Fig. 2(d), where correlations between propagating modes in the up- and downstream regions (including the Hawking mustache) lay. As shown in Fig. 4, the FT of real data yields a pair of symmetric spectral lines centered in $k_{u,d} = 0$. These lines follow the locus of $k_{u,d}$ spanned by the dispersion of modes $u_{out} - d2_{out}$ (orange line) and $u_{out} - d1_{out}$ (blue line) as a function of ω. As anticipated in [48,49], this is the characteristic signature of the HE in k space. While they are well separated at large $k_{u,d}$, the tongues merge at low $k_{u,d}$ because of the limited size of the sampling box and the further spectral broadening due to the finite life-time of Bogoliubov excitations. The spectral lines are cut off at small $k_{u,d}$ corresponding to the ω_{min} gap in the dispersion in the upstream region, and extend to large $k_{u,d}$ corresponding to ω_{max} in the downstream region.

Most importantly, beyond ω_{max}, the emission spectrum shows an additional peak at $0.78(3)$ μm^{-1}, $0.25(3)$ μm^{-1} in the $k_{u,d}$ plane. Within the uncertainty due to the numerical grid size in Fig. 4, these coordinates correspond to the wave numbers extracted previously for the ringdown at frequency ω_{QNM}. This nontrivial structure of the spectrum is at the origin of the additional fringes next to the Hawking mustache indicated as feature (v) in Fig. 2(d). So this peak highlights a sizable additional contribution to
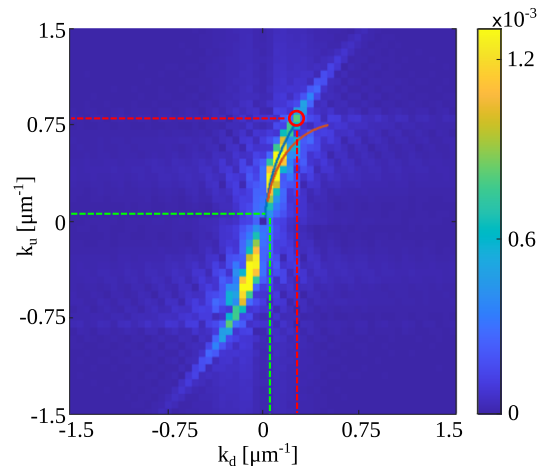
FIG. 4. Hawking emission spectrum. Two-dimensional FT of $g^{(2)}(x, x')$ within the black rectangle in the up-downstream region in Fig. 2(d). Orange line, analytical locus of u_{out}-$d2_{out}$ correlations; Blue line, analytical locus of u_{out}-$d1_{out}$ correlations. Green dotted line, wavenumber cutoff $k_u = 0.03(3)$ μm^{-1} and $k_d = 0.01(3)$ μm^{-1} [due to the low-frequency gap in upstream dispersion, cf. Fig. 2(a)]; Red dotted line, wave numbers of the propagating component of the QNM $k_u = 0.78(3)$ μm^{-1} and $k_d = 0.25(3)$ μm^{-1}.

the u_{out}-$d1_{out}$ correlations that are normally quite weak and indicates the spectral modulation of the HE by the quantum-fluctuation-driven excitation of the QNM. A similar peak is visible in the HE spectrum in conservative fluids as well (see SM), although the peak there is located at a frequency $\omega_{QNM} < \omega_{max}$. This indicates that the effective resonator acts as a frequency filter for the Hawking spectrum, i.e., a gray-body factor.

Conclusions.—In this Letter, we have made use of an effectively curved spacetime realized in a polariton fluid to theoretically show that vacuum quantum fluctuations near a sonic horizon do not only yield the correlated emission of propagating waves by the Hawking effect but also cause a stationary quantum excitation of a quasinormal mode of the acoustic field. Specific features of this process are visible both in the correlation diagram of density fluctuations and in the spectrum of the Hawking emission. Since our calculations are performed with experimental parameters and give a strong signal, the effects are amenable to experimental observation with state-of-the-art technology. Although the microscopic origin of the decaying QNM mode may differ in driven-dissipative and conservative quantum fluids, similar signatures of the vacuum excitation of the QNM are visible in both cases. This suggests that our conclusions are valid for generic quantum fluids.

But the generality of the vacuum excitation of QNMs goes even beyond analog models. Indeed, it originates in basic processes of quantum field theory in effectively curved spacetimes whose equivalence with Klein-Gordon fields on black-hole spacetimes is well established [4,5]. For example, resonance peaks in the Hawking spectrum of astrophysical black holes appear via gray-body factors [50] and are associated with unstable orbits [51]. In the quantum fluid configuration studied here, the resonator is located inside the horizon. This is possible because of the specific superluminal dispersion of the fluid. However, this needs not be the case in general—similar physics can be observed with resonators outside the horizon. In astrophysical black holes, the localized component of the QNM is supported in the region between the light ring and the horizon and its amplitude naturally damps via radiative decay into propagating waves. This suggests that our conclusions directly extend to the gravitational context, so that all quantum fields in curved spacetimes would exhibit the effects predicted in this work. As such, the enhanced quantum fluctuations of the field in the localized component of QNMs raise questions on the role of their associated entropy [52–54] and on the intrinsic fluctuations of black-hole spacetimes.

*Corresponding author.
 maxime.jacquet@lkb.upmc.fr

[1] S. W. Hawking, Nature (London) **248**, 30 (1974).
[2] C. Barceló, S. Liberati, and M. Visser, Living Rev. Relativity **14**, 3 (2011).
[3] M. J. Jacquet, S. Weinfurtner, and F. König, Phil. Trans. R. Soc. A **378**, 20190239 (2020).
[4] W. G. Unruh, Phys. Rev. Lett. **46**, 1351 (1981).
[5] M. Visser, Classical Quantum Gravity **15**, 1767 (1998).
[6] T. G. Philbin, C. Kuklewicz, S. Robertson, S. Hill, F. König, and U. Leonhardt, Science **319**, 1367 (2008).
[7] G. Rousseaux, C. Mathis, P. Maïssa, T. G. Philbin, and U. Leonhardt, New J. Phys. **10**, 053015 (2008).
[8] O. Lahav, A. Itah, A. Blumkin, C. Gordon, S. Rinott, A. Zayats, and J. Steinhauer, Phys. Rev. Lett. **105**, 240401 (2010).
[9] S. Weinfurtner, E. W. Tedford, M. C. J. Penrice, W. G. Unruh, and G. A. Lawrence, Phys. Rev. Lett. **106**, 021302 (2011).
[10] J.-C. Jaskula, G. B. Partridge, M. Bonneau, R. Lopes, J. Ruaudel, D. Boiron, and C. I. Westbrook, Phys. Rev. Lett. **109**, 220401 (2012).
[11] H. S. Nguyen, D. Gerace, I. Carusotto, D. Sanvitto, E. Galopin, A. Lemaître, I. Sagnes, J. Bloch, and A. Amo, Phys. Rev. Lett. **114**, 036402 (2015).
[12] T. Torres, S. Patrick, A. Coutant, M. Richartz, E. W. Tedford, and S. Weinfurtner, Nat. Phys. **13**, 833 (2017).
[13] S. Eckel, A. Kumar, T. Jacobson, I. B. Spielman, and G. K. Campbell, Phys. Rev. X **8**, 021021 (2018).
[14] D. Vocke, C. Maitland, A. Prain, K. E. Wilson, F. Biancalana, E. M. Wright, F. Marino, and D. Faccio, Optica **5**, 1099 (2018).
[15] M. Wittemer, F. Hakelberg, P. Kiefer, J.-P. Schröder, C. Fey, R. Schützhold, U. Warring, and T. Schaetz, Phys. Rev. Lett. **123**, 180502 (2019).
[16] L.-P. Euvé, S. Robertson, N. James, A. Fabbri, and G. Rousseaux, Phys. Rev. Lett. **124**, 141101 (2020).
[17] M. J. Jacquet, T. Boulier, F. Claude, A. Maître, E. Cancellieri, C. Adrados, A. Amo, S. Pigeon, Q. Glorieux, A. Bramati, and E. Giacobino, Phil. Trans. R. Soc. A **378**, 20190225 (2020).
[18] S. Patrick, H. Goodhew, C. Gooding, and S. Weinfurtner, Phys. Rev. Lett. **126**, 041105 (2021).
[19] R. Balbinot, A. Fabbri, S. Fagnocchi, A. Recati, and I. Carusotto, Phys. Rev. A **78**, 021603(R) (2008).
[20] I. Carusotto, S. Fagnocchi, A. Recati, R. Balbinot, and A. Fabbri, New J. Phys. **10**, 103001 (2008).
[21] L.-P. Euvé, F. Michel, R. Parentani, T. G. Philbin, and G. Rousseaux, Phys. Rev. Lett. **117**, 121301 (2016).
[22] J. R. Muñoz de Nova, K. Golubkov, V. I. Kolobov, and J. Steinhauer, Nature (London) **569**, 688 (2019).
[23] D. D. Solnyshkov, H. Flayac, and G. Malpuech, Phys. Rev. B **84**, 233405 (2011).

[24] D. Gerace and I. Carusotto, Phys. Rev. B **86,** 144505 (2012).

[25] P. Grišins, H. S. Nguyen, J. Bloch, A. Amo, and I. Carusotto, Phys. Rev. B **94,** 144518 (2016).

[26] M. Jacquet, M. Joly, F. Claude, L. Giacomelli, Q. Glorieux, A. Bramati, I. Carusotto, and E. Giacobino, Eur. Phys. J. D **76,** 152 (2022).

[27] S. Chandrasekhar and S. Detweiler, Proc. R. Soc. A **344,** 441 (1975).

[28] E. Berti, V. Cardoso, and A. O. Starinets, Classical Quantum Gravity **26,** 163001 (2009).

[29] A. Coutant, F. Michel, and R. Parentani, Classical Quantum Gravity **33,** 125032 (2016).

[30] T. Torres, S. Patrick, M. Richartz, and S. Weinfurtner, Phys. Rev. Lett. **125,** 011301 (2020).

[31] I. Zapata, M. Albert, R. Parentani, and F. Sols, New J. Phys. **13,** 063048 (2011).

[32] A. Baas, J. P. Karr, H. Eleuch, and E. Giacobino, Phys. Rev. A **69,** 023809 (2004).

[33] I. Carusotto and C. Ciuti, Rev. Mod. Phys. **85,** 299 (2013).

[34] I. Amelio and I. Carusotto, Phys. Rev. B **101,** 064505 (2020).

[35] J. Macher and R. Parentani, Phys. Rev. D **79,** 124008 (2009).

[36] A. Recati, N. Pavloff, and I. Carusotto, Phys. Rev. A **80,** 043603 (2009).

[37] S. Corley and T. Jacobson, Phys. Rev. D **54,** 1568 (1996).

[38] M. Jacquet and F. König, SciPost Phys. Core **3,** 005 (2020).

[39] I. Carusotto and C. Ciuti, Phys. Rev. B **72,** 125335 (2005).

[40] See Supplemental Material at http://link.aps.org/supplemental/10.1103/PhysRevLett.130.111501 for the numerical methods and parameters for numerical calculations. Detailed analysis of the ringdown data and extraction of QNM frequency from correlations. Diagonalization of the inhomogeneous Bogoliubov problem. Numerical calculations showing the excitation of a QNM in a conservative fluid.

[41] LIGO Scientific and Virgo Collaborations, Phys. Rev. Lett. **116,** 061102 (2016).

[42] L. Giacomelli and I. Carusotto, Phys. Rev. Res. **2,** 033139 (2020).

[43] C. L. Tang and L. K. Cheng, *Fundamentals of Optical Parametric Processes and Oscillators*, Laser Science and Technology, Vol. 20 (Harwood Academic Publishers, Amsterdam, 1995).

[44] J. Steinhauer, Phys. Rev. D **92,** 024043 (2015).

[45] S. Robertson, F. Michel, and R. Parentani, Phys. Rev. D **96,** 045012 (2017).

[46] M. Isoard and N. Pavloff, Phys. Rev. Lett. **124,** 060401 (2020).

[47] M. Isoard, N. Milazzo, N. Pavloff, and O. Giraud, Phys. Rev. A **104,** 063302 (2021).

[48] D. Boiron, A. Fabbri, P.-E. Larré, N. Pavloff, C. I. Westbrook, and P. Ziń, Phys. Rev. Lett. **115,** 025301 (2015).

[49] A. Fabbri and N. Pavloff, SciPost Phys. **4,** 019 (2018).

[50] D. N. Page, Phys. Rev. D **14,** 3260 (1976).

[51] C. Goebel, Astrophys. J. **172,** L95 (1972).

[52] J. W. York, Phys. Rev. D **28,** 2929 (1983).

[53] S. Hod, Phys. Rev. Lett. **81,** 4293 (1998).

[54] M. Maggiore, Phys. Rev. Lett. **100,** 141301 (2008).